POOJA, PANCHOLI, K. and DWIVEDI, Y. 2024. Tailoring optical properties and humidity sensing response of multilayered Tb(Sal)3Phen and Eu(DBM)3Phen complex nanofibres. *Optical materials: X* [online], 23, article number 100340. Available from: https://doi.org/10.1016/j.omx.2024.100340

Tailoring optical properties and humidity sensing response of multilayered Tb(Sal)3Phen and Eu(DBM)3Phen complex nanofibres.

POOJA, PANCHOLI, K. and DWIVEDI, Y.

2024

OpenAIR @RGU

This document was downloaded from https://openair.rgu.ac.uk

CC BY NC ND

Optical Materials: X 23 (2024) 100340

Contents lists available at ScienceDirect

Optical Materials: X

journal homepage: www.journals.elsevier.com/optical-materials-x

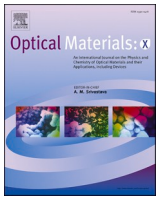

Tailoring optical properties and humidity sensing response of multilayered $Tb(Sal)_3Phen$ and $Eu(DBM)_3Phen$ complex nanofibres

Pooja [a], Ketan Pancholi [b], Yashashchandra Dwivedi [a,*]

[a] Department of Physics, National Institute of Technology, Kurukshetra, India
[b] School of Engineering, Robert Gordon University, Aberdeen, AB10 7GJ, UK

ARTICLE INFO

Keywords:
Spectroscopy
Electrospinning
Nanofibres
Humidity response

ABSTRACT

In this work, we investigate the opto-humidity sensing and colour tuning in polyvinyl alcohol (PVA) polymeric electrospun nanofibres dispersed with $Tb(Sal)_3Phen$ (TSP) and $Eu(DBM)_3Phen$ (EDP) complexes. Fourier transform infrared spectroscopy, scanning electron microscopy, and photoluminescence analysis were used to thoroughly analyse the structural, morphological, and spectroscopic features of the synthesised nanofibres in single and stacked multilayer nanofibres. A spectroscopic analysis was performed on all configuration schemes. Under UV excitations, the synthesised TSP complex and EDP complex inhibited nanofibres yield green and red emission corresponding to $^5D_4 \rightarrow {}^7F_j$ (j = 4, 5, 6) and $^5D_0 \rightarrow {}^7F_j$ (j = 0, 1, 2, 3) transitions attributed to Tb^{3+} and Eu^{3+} ions, respectively. The EDP nanofibres presented better UV radiation absorption than TSP, which was attributed to higher absorptivity of DBM than Sal. Additionally, the photoluminescence intensity ratio of characteristic emission peaks i.e. 544 nm ($^5D_4 \rightarrow {}^7F_5$)/615 nm ($^5D_0 \rightarrow {}^7F_2$) is function of humidity exposure and excitation wavelength. The stacked multilayer nanofibres exhibit good response and recovery times, 35 and 52 s, negligible hysteresis, and cyclic stability.

1. Introduction

Humidity sensing plays a crucial role in various fields in maintaining comfortable and healthy environments, as well as ensuring optimal performance and safety in industrial processes. The ability to accurately measure and monitor humidity levels helps in understanding and controlling moisture content, preventing issues such as mold growth, corrosion and degradation of materials. Additionally, maintaining specific humidity conditions is critical for product quality and safety in fields like pharmaceuticals, food processing, storage facilities, etc. Opto-humidity sensors are one of the key devices used for humidity measurement. They provide reliable and real-time data on humidity levels, allowing for precise control and adjustment of environmental conditions. These sensors offer advantages such as fast response time, high accuracy, and long-term stability. The development of advanced opto-humidity sensors continues to enhance our ability to monitor and regulate humidity, contributing to improved comfort, productivity, and overall well-being [1–3]. Electrospun nanofibres are a promising material for humidity sensors due to their large surface area, porosity, and ability to be dispersed with a variety of ions/molecules. Humidity sensors based on electrospun nanofibres can detect changes in relative humidity by measuring the electrical resistance or capacitance or the optical response of the active nanofibres mat. The sensitivity and response time of the sensors depend on various factors, such as the composition, morphology, and alignment of the nanofibres, as well as the fabrication and integration methods. The polymeric electrospun nanofibres dispersed with humidity-responsive organic molecules like lanthanide complexes have gained significant attention as opto-humidity sensors due to their rapid optical response, flexible composition, optical excitation, etc. The electrospinning technique enables the production of lanthanide complex-doped nanofibres with controlled morphology and composition. Lanthanide (Ln) complexes possess broad UV/blue excitations (due to the presence of ligands in the complex) and the sharp emission of Ln ions.

The optical properties of Ln complexes are reported to be a function of humidity in the microenvironment. This is because the water molecules in the ambience affect the energy levels, so the radiative transitions in the lanthanide ions alter their colour, lifetime and intensity. Lanthanide complex-based moisture sensors have improved sensitivity, stability, and applicability [4]. For example, Gonzalez et al. synthesised Eu^{3+} and Tb^{3+} complexes using 8-Methoxy-4,5-dihydrocyclopenta[de] quinolin-2(1H)-one phosphonates or carboxylates and quinolin-2

* Corresponding author.
E-mail address: yashjidwivedi@nitkkr.ac.in (Y. Dwivedi).

https://doi.org/10.1016/j.omx.2024.100340
Received 12 December 2023; Received in revised form 27 June 2024; Accepted 2 July 2024
Available online 14 July 2024
2590-1478/© 2024 The Author(s). Published by Elsevier B.V. This is an open access article under the CC BY-NC-ND license (http://creativecommons.org/licenses/by-nc-nd/4.0/).

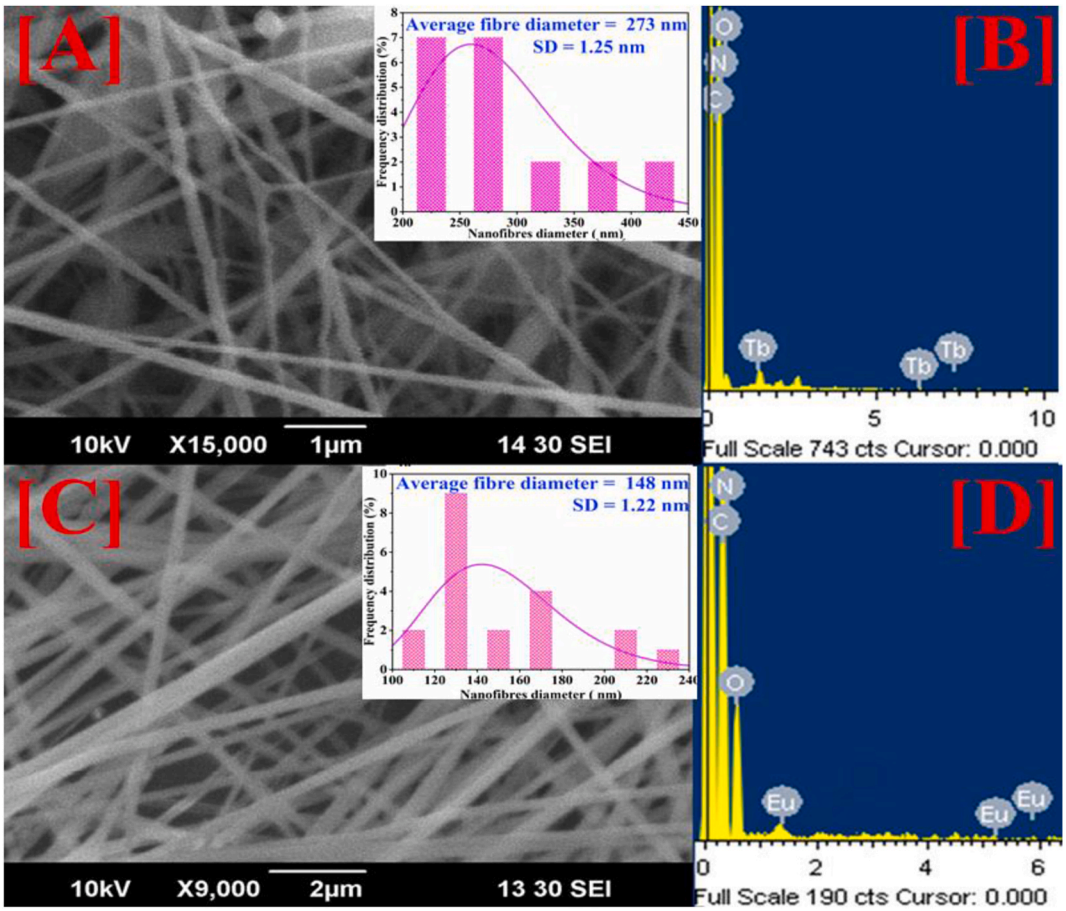

Fig. 1. Scanning electron microscope (SEM) images and corresponding histograms (inset) for (A) TSP and (C) EDP nanofibres. EDS spectra of (B) TSP and (D) EDP nanofibres.

(1H)-one for sensing traces of H_2O in organic solvents [5], Gao et al. combined photoluminescence and impedance spectroscopy studies for synthesising europium based MOF i.e. $[Eu(H_2O)_2(mpca)_2Eu(H_2O)_6M(CN)_8].nH_2O$ (where mpca = 2-pyrazine-5-methyl-carboxylate, M = Mo, W) for dual-mode humidity detection [6] and Pooja et al. synthesised Tb:Ce$(Sal)_3$Phen complex dispersed PVA nanofibre for flexible moisture sensing [7]. The luminescent response of the lanthanide ions is typically sharp and easily detectable, allowing for accurate monitoring of humidity levels [8]. Additionally, lanthanide complexes can be tailored to exhibit specific luminescent properties, enabling the development of sensors with customized detection ranges. Moreover, the electrospun nanofibres offer several benefits, such as a large surface-to-volume ratio, fast response time, and flexibility [9]. These features enable efficient moisture absorption and desorption, ensuring rapid and reversible sensing performance. The on-going research and development in this area aims to optimize the sensor performance, stability, and durability, further expanding their applications in humidity sensing and related fields [7,9]. The operating principles of opto-humidity sensors are mostly Ratiometric Sensors, Chromogenic Sensors, Surface Acoustic Wave Sensors, Surface Plasmon Resonance Sensors, Impedance-based Sensors, etc. [10–14]. The ratiometric method is preferred because it provides internal reference and facilitates good reproducibility. The presence of neutral ions for internal referral in the same lattice with the humidity-responsive active ion may interfere, leading to poor sensing performance. It is suggestive that, to minimize the interaction, the humidity-sensitive and insensitive species may be kept in isolated layers.

To serve the purpose of least interference of neutral ion on humidity response, we fabricated two humidity-sensitive polyvinyl alcohol (PVA) nanofibres mats; one nanofibres mat was dispersed with Eu$(DBM)_3$Phen complex, while the second was dispersed with humidity-sensitive-Tb $(Sal)_3$Phen complex. We report the opto-humidity variation with different stacking of layers. The PVA nanofibres matrix serves as a porous host with a large surface area and humidity-capturing network, which enhances the sensitivity towards ambient humidity. Trivalent Tb and Eu ions are enriched with dense energy levels, which yield blue-green ($Tb^{3+)}$ and yellow-red (Eu^{3+}) colours. However, when these two ionic species are in the same matrix, they interact via energy transfer (Eu^{3+} to Tb^{3+}ion). Such interaction leads to a significant reduction in blue/green emission while increasing red emission. It is interesting to note that these two ionic species emit primary colours, which is required for high-contrast display devices.

In the present article, to avoid interactions between the doped species, without compromising the emission characteristics and to have precise control over the emission intensity, we fabricated two different electrospun nanofibres and staked them (one on one). We monitor the optical response of the mat in different humidity conditions and report the same.

2. Synthesis and characterization

All chemicals with high purity were purchased from Sigma-Aldrich Company for synthesis and used as received. Briefly, Tb$(Sal)_3$Phen was synthesised using, Terbium (III) chloride hexahydrate, Salicylic acid and, 1,10-phenanthroline (Phen), following the method reported previously [15]. Similarly, Eu$(DBM)_3$Phen was synthesised using Dibenzoylmethane (DBM), Europium chloride (III), and 1,10-Phenonthroline as a starting material, following the method reported in Ref. [16]. The synthesis of Tb$(Sal)_3$Phen complex yielded light orange-brown coloured

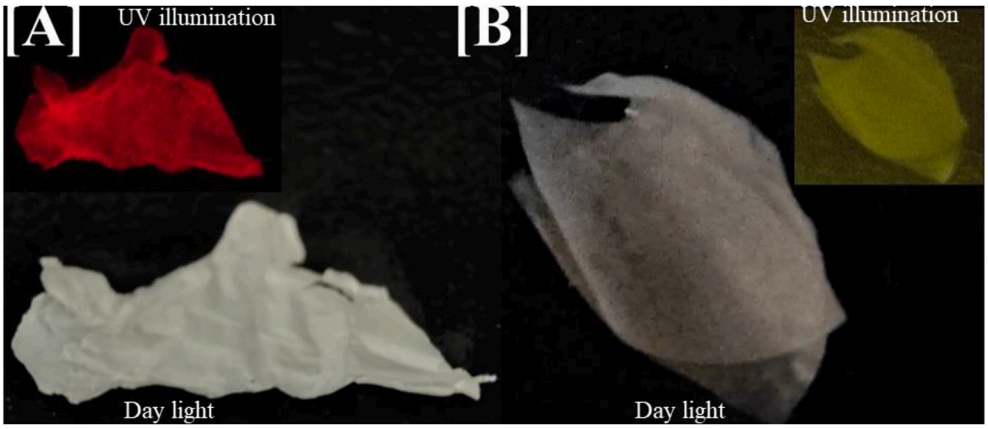

Fig. 2. The daylight UV-C illumination images of [A] EDP and [B] TSP nanofibres.

crystals whereas $Eu(DBM)_3Phen$ resulted in a pale yellow powder. These products were carefully collected for subsequent measurements. The complex $Tb(Sal)_3Phen$ will be referred TSP and complex $Eu(DBM)_3Phen$ will be referred EDP in throughout the remaining text.

2.1. Fabrication of nanofibres

For the fabrication of nanofibres, 7 % w/w of the PVA solution was obtained by dissolving an appropriate amount of Polyvinyl alcohol (PVA, Mw - 85,000 – 125,000) in warm (80 °C) double distilled water. The weight ratio of PVA to TSP and EDP complex was 1:0.01. The mixture was stirred until a uniform solution was obtained. The 1 ml syringe used in the electrospinning setup (E-spin Nanotech Company, India) was filled with the previous prepared solution to spin the nanofibres on aluminium covered collector. During the spinning of nanofibres, the tip-to-collector distance was kept constant at 14 cm, while static DC voltage supplied was kept at 15 kV. The solution flow rate of 0.05 ml/h was maintained throughout.

2.2. Characterisations

The synthesised TSP and EDP nanofibres were examined using a scanning electron microscopy (SEM) (JEOL JSM-6390LV) fitted with energy dispersive X-ray spectroscopy (EDS) apparatus to determine their surface shape and elemental composition. Using a PerkinElmer Spectrum 65 FTIR spectrometer, Fourier transform infrared absorption spectra were obtained in the 500-4000 cm^{-1} spectral region with a resolution of 1 cm^{-1}. FTIR spectra were monitored in Attenuated total reflection (ATR) mode. Using Xenon lamp as excitation source, the photoexcitation and luminescence spectra of the TSP and EDP complex nanofibres were captured at room temperature using the SHIMADZU RF-530 spectrometer. At room temperature the multilayer's emission intensity change was also noted. The colour images were observed under UV-C light exposure of the samples. We monitored the humidity response emission characteristic in a customized acrylic box, while keeping it inside the SHIMADZU RF-530 spectrometer. This box has an inlet and an outlet nozzle attached with vacuum pump and N_2 gas cylinder. The 288-CTH hygrometer measuring humidity in the range 10 %–99 % RH with an accuracy of ±5 % was used for measuring the moisture

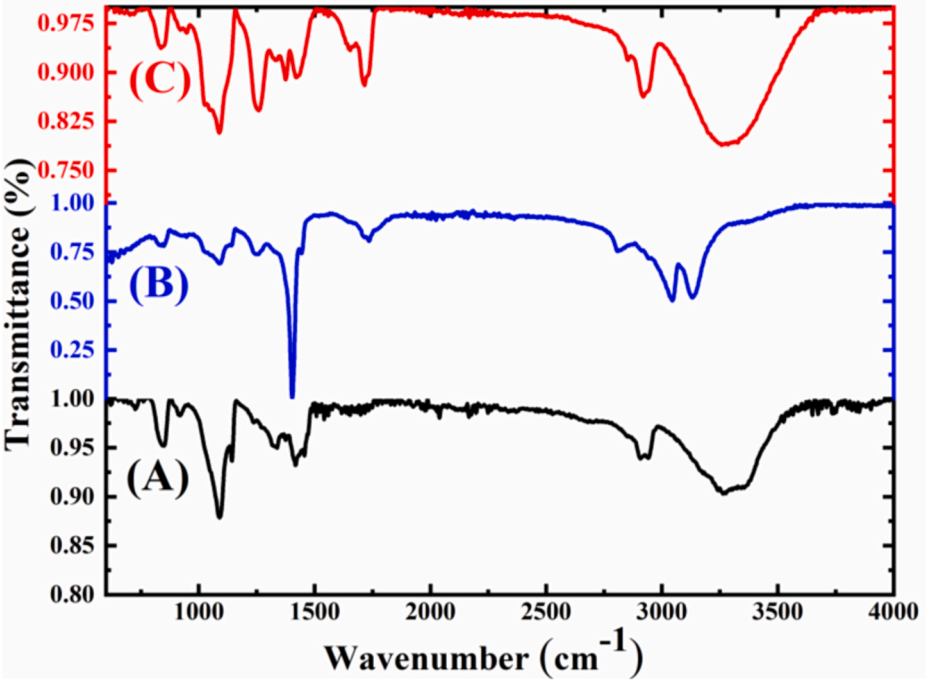

Fig. 3. FTIR spectra of (A) $Eu(DBM)_3Phen$, (B) $Tb(Sal)_3Phen$, (C) pure PVA nanofibres.

content, which is placed inside the box with sample holder.

3. Results and discussion

3.1. Morphological and optical analysis

The SEM images of the synthesised PVA nanofibres integrated with TSP and EDP complexes are shown in Fig. 1. The fibrous structure of both the nanofibres is observed from the SEM images. The frequency distribution histograms of both the nanofibres layers were plotted using the normal distribution curve; the average fibre diameter was determined from the histograms and found to be ~273 ± 1.25 nm and ~148 ± 1.22 nm for TSP and EDP nanofibres, respectively with the length > 1 mm. The narrower diameter distribution of TSP nanofibres suggests a more uniform production process compared to EDP nanofibres. The EDS (energy dispersive X-ray) spectrum for the nanofibres is given in Fig. 1 [B], [D]. The EDS spectrum for TSP exhibited the spectral peaks related to Tb, C, N and O elements due to the presence of ions of terbium, Salicylic acid, Phenanthroline and polymer PVA. The EDS spectrum of EDP nanofibres showed the presence of Eu, C, N and O elements corresponding to Europium, Phenanthroline, Dibenzoylmethane and PVA polymer. No foreign spectral peaks were found in the EDX spectrum. Subsequently, the nanofibres were examined for optical properties.

Both the nanofibres layers were viewed under UV-C lamp illumination. Fig. 2 display the images under daylight and UV illumination, showing the EDP nanofibres sheet with red emission and TSP nanofibres with green emission.

3.2. Fourier transform infrared analysis

To study the molecular vibrations of the nanofibres, the infrared absorption spectra were obtained for all the samples given in Fig. 3. Pure PVA nanofibres (Fig. 3 (C)) FTIR spectrum exhibited the molecular vibrations attributed to C–H bond at 844 cm^{-1} and the C–O vibrations at 1092 cm^{-1} and 1260 cm^{-1}. The band at 1374 cm^{-1} arises from CH–OH vibrations. Other vibrational bands at 1429 and 2925 cm^{-1} are assigned to CH_2 symmetric and anti-symmetric stretching in the PVA. The band at 1724 cm^{-1} is due to the stretching vibrations of C═O groups of the remaining vinyl acetate repeating units of PVA. The bands corresponding to $–CH_2$, $–CH_3$, and O–H stretching vibrations in the TSP nanofibres (Fig. 3 [B]) are the observed between 2500 cm^{-1} and 3500 cm^{-1}. The salicylic acid's characteristic bands are observed at 1445 cm^{-1} (C–C stretching) and 1388 cm^{-1} (salicylic acid's OCO-symmetric stretching) [17]. Band at 852 cm^{-1} for TSP are assigned CH out-of-plane deformation owing to Phenanthroline ring [18], whereas bands at 1020 cm^{-1} and 1071 cm^{-1} are due to ring CH vibrations [19].

The bands at 1085 cm^{-1} and 928 cm^{-1} correspond to distinctive C–O stretching and CH_2 rocking vibrations of PVA polymer [20]. In the FTIR spectrum of $Eu(DBM)_3Phen$ (Fig. 3 [A]), the vibrational bands corresponds to PVA nanofibres along with the vibrations in between 1410 and 1600 cm^{-1} attributed to the stretching vibrations of C–O, C–C and C–N of DBM and Phen. The band at 2911 cm^{-1} corresponds to CH–CH stretching vibrations of phenyl derivatives and the vibrations in the region 3000-3500 cm^{-1} can be attributed to the intramolecularly bound carboxylic group [21]. The FTIR spectrum of the PVA incorporated complex nanofibres ($Eu(DBM)_3Phen$ and $Tb(Sal)_3Phen$) were mostly dominated by the vibrational peaks of the PVA nanofibres and some minor peaks corresponding to the complex molecular vibrations. This is owing to a small complex to PVA polymer in the nanofibres (in a ratio 1: 0.01).

3.3. Optical analysis

The excitation and emission spectra of the complex nanofibres were monitored to investigate potential spectroscopic changes in the single and bilayer systems attributable to interlayer energy interactions.

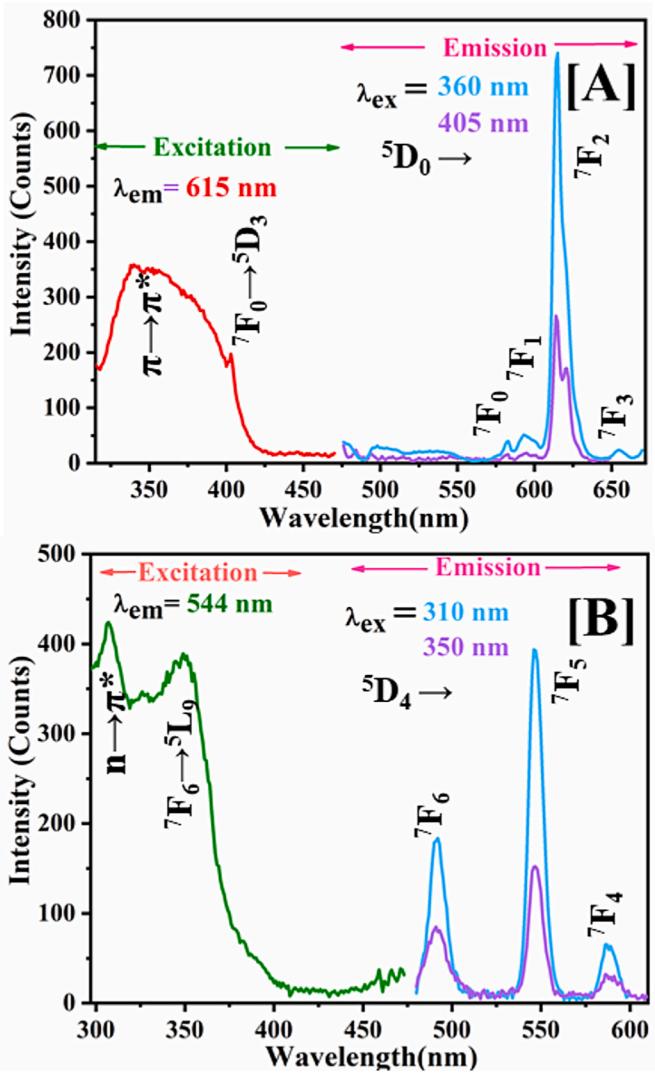

Fig. 4. Excitation and emission spectra of [A] EDP and [B] TSP single layer nanofibres placed on aluminium substrate.

Afterwards, the variation in emission intensity and humidity sensing characteristics of the bilayer system in two configurations were investigated.

3.3.1. Optical analysis of single layer $Eu(DBM)_3Phen$ and $Tb(Sal)_3Phen$ on aluminium substrate

The $Eu(DBM)_3Phen$ nanofibres were electrospun on aluminium substrate to obtain emission and excitation spectra as shown in Fig. 4 [A]. The emission spectrum of the single sheet of EDP fibre was monitored for the most intense emission peak of Eu^{3+} at 615 nm corresponding to the transition $^5D_0 \rightarrow {}^7F_2$.The excitation spectra consisted of broad band ranging from 315 nm to 410 nm corresponding to the absorption of the DBM ligand and a small hump at 405 nm attributable to direct excitation of Eu^{3+} ion. The emission spectra was obtained for excitation wavelengths 360 nm and 405 nm corresponding to the absorption DBM and europium ion, respectively. The emission spectra consisted of peaks at 581 nm, 593 nm and 615 nm are attributed to the $^5D_7 \rightarrow F_j$ (j = 0–3) transitions. From the spectrum in Fig. 4 [A], it is observed that the maximum emission intensity yields from absorption wavelength corresponding to DBM (360 nm) due to energy transfer from the ligand DBM to Eu^{3+} [21].

The $Tb(Sal)_3Phen$ nanofibres were fabricated on aluminium substrate and examined for photoluminescence spectra (PL) as shown in

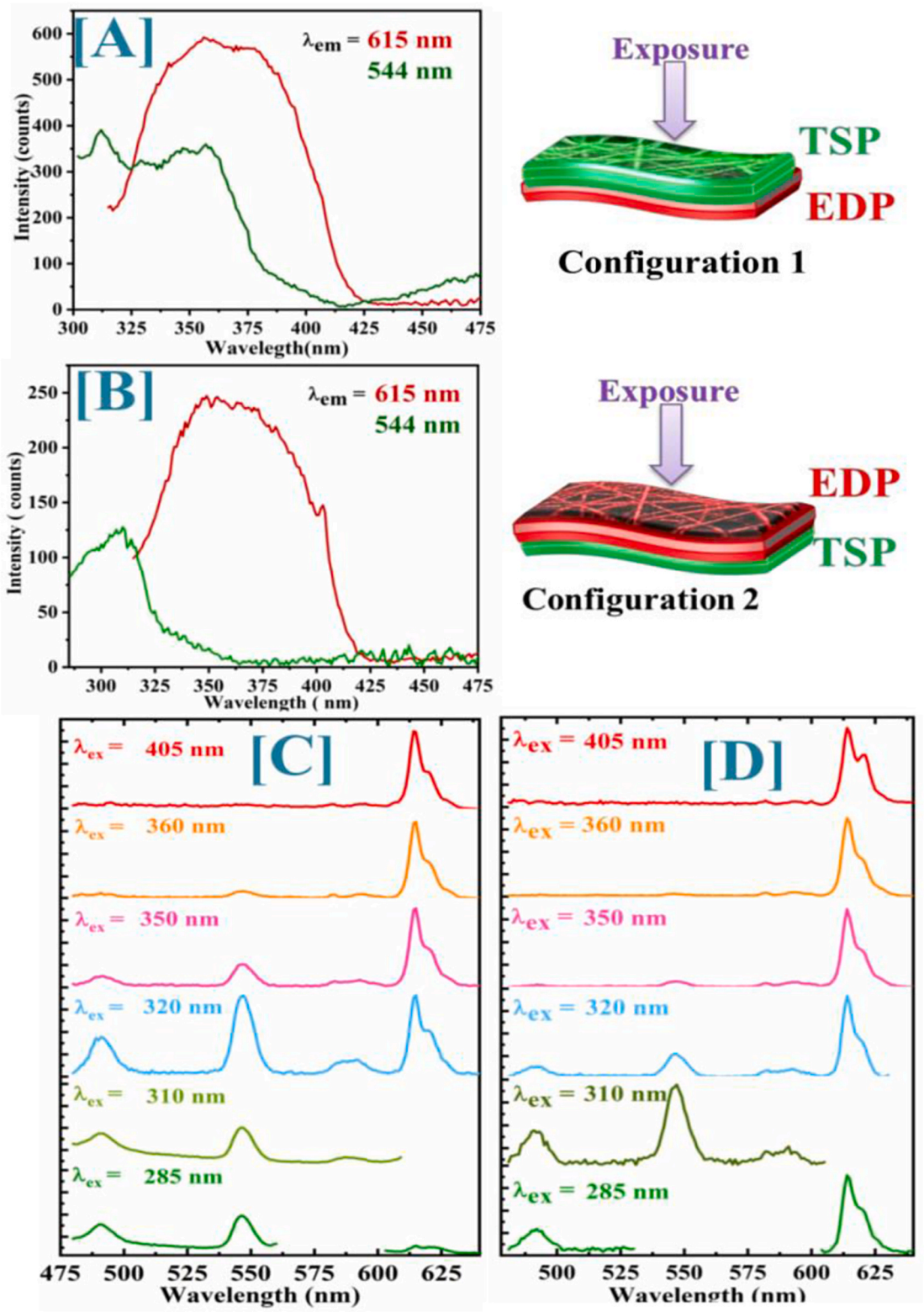

Fig. 5. Excitation spectra of [A] configuration-1 and [B] configuration-2. The emission spectra of [C] configuration-1 and [D] configuration-2 along with pictorial representation of the configurations.

Fig. 4[B]. For the excitation spectra the emission wavelength was kept at 544 nm as it is the most intense peak corresponding to Tb^{3+} ion. The excitation spectra consisted of two bands one centred on 310 nm corresponding to n→π* transitions of coordinated Salicylate ion. And other centred at 350 nm due to absorption of Tb^{3+} ion. The emission spectra were monitored for excitation wavelengths 310 nm and 350 nm corresponding to absorption of salicylate anion and Tb^{3+}. The emission spectra consisted of peaks due to $^5D_4 \rightarrow {}^7F_6$ (490 nm), $^5D_4 \rightarrow {}^7F_5$ (544 nm), $^5D_4 \rightarrow {}^7F_4$ (580 nm) transitions of Tb^{3+} ion. The maximum emission intensity was found for excitation wavelength 310 nm due to intramolecular energy transfer from salicylate ion to Tb^{3+} ion [15].

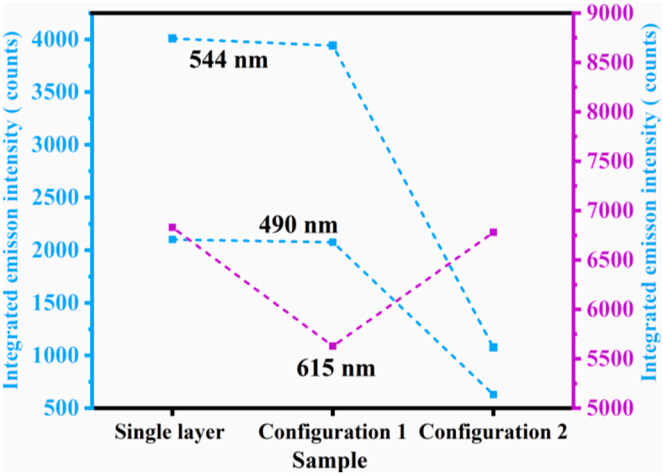

Fig. 6. Plots showing the variation of the integrated emission intensity of the nanofibres layer in single layer and different configuration of multilayer.

3.3.2. *Optical analysis of stacked multilayer mat*

The alterations in spectroscopic properties in a multilayer system compared to a single layer of nanofibres were examined, and the light modulation in the different configurations of the multilayer system was also studied. The PL spectra of the multilayer nanofibres system were monitored, and corresponding emission and excitation spectra were plotted. Firstly, emission was recorded for the configuration-1: the TSP nanofibres layer was kept over the EDP layer.

The excitation spectra were monitored for emission wavelengths 544 nm and 615 nm (Fig. 5 [A], [B]). The excitation spectra for the emission wavelength 544 were similar to single layer spectra with characteristic band at 310 nm corresponding to the absorption of salicylate ion. In the excitation spectra for configuration-2, EDP layer is blocking significant portion of the light to reach the bottom TSP layer. However, when the configuration is reversed i.e. TSP layer is placed on top, the layer did not absorb significant portion of incident energy as if we compare the absorbance of organic ligands in two layers i.e. DBM and Sal, DBM has higher molar absorptivity (2.6×10^4 $M^{-1}cm^{-1}$) [22] than the Sal (3.8×10^3 $M^{-1}cm^{-1}$) molecule [23,24]. For the emission wavelength 615 nm, a broad emission ranging from 315 nm to 405 nm was observed, corresponding $\pi \rightarrow \pi^*$ in the ligand DBM, along with a shoulder peak at 405 nm attributed to the absorption of Eu^{3+} ion. The multilayer system was subjected to all possible excitation wavelengths to observe the light modulation through the variation in intensity corresponding to the ions Tb^{3+} and Eu^{3+}. From the emission spectra it can be observed that when exciting the multilayer with 285 nm yields blue-green emission of Tb^{3+} and red emission of Eu^{3+}. The maximum yield of green blue emission of Tb^{3+} was observed for excitation 310 nm and upon increasing the excitation wavelength further the blue green emission of Tb^{3+} gradually decreased and red emission ascribed to Eu^{3+} enhanced until 370 nm. At 405 nm the spectrum consists of only red emission due to Eu^{3+} ions. It was observed that at 320 nm excitation the emission spectrum consisted of both green blue and red emission with comparable intensities. Hence, the emission from the multilayer system can be modulated between blue green to red colour with different proportion of the two colours. Fig. 5 [A] and [C] represents the excitation and emission spectrum for configuration-1 i.e. when TSP nanofibres layer was on top of EDP. For this configuration, emission peaks corresponding to Tb^{3+} and Eu^{3+} ions were similar to the ones obtained in

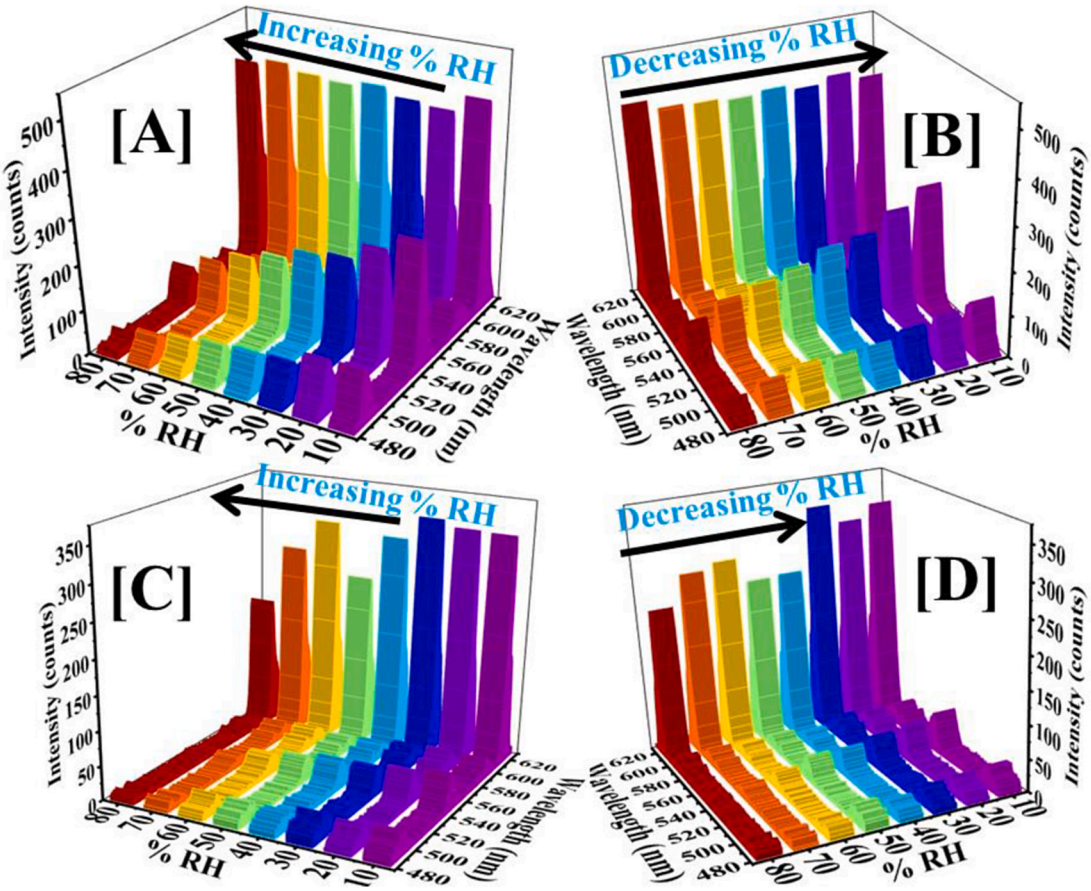

Fig. 7. Photoluminescence spectra of the multilayer nanofibres of configuration-1 for [A] decreasing and [B] increasing RH (unit%); configuration-2 for [C] decreasing and [D] increasing RH (unit%).

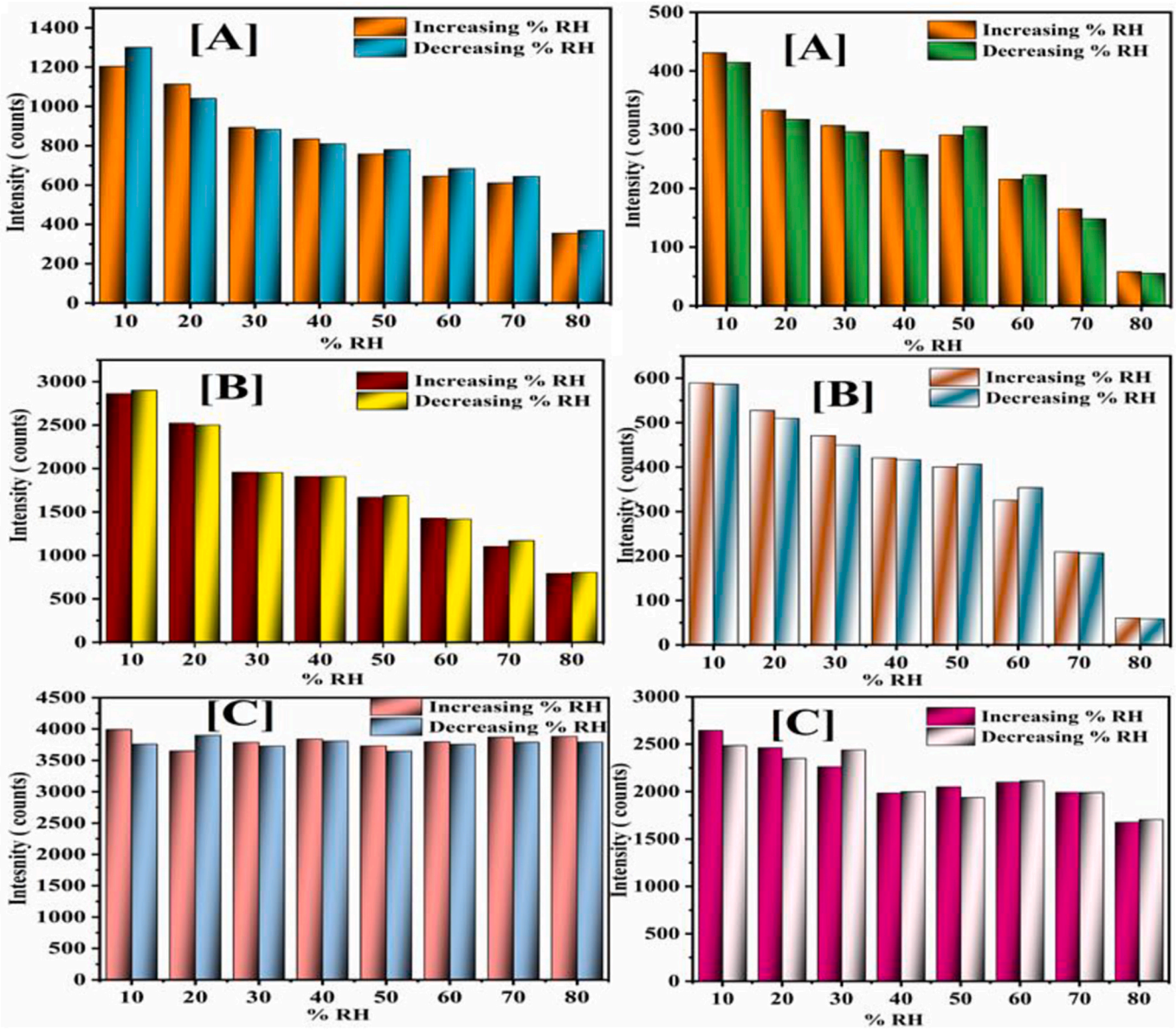

Fig. 8. The hysteresis curve for configuration-1 (left) and configuration-2 (right) for [A] 490 nm, [B] 544 nm and [C] 615 nm.

configuration-2 but with an enhancement in Tb^{3+} ion emission intensity (see Fig. 6).

To study the spectroscopic changes in the emission intensity of the single nanofibre layer and the same layer when incorporated into the multilayer system, the integrated emission intensity (peak area) of the 544 nm and 490 nm (TSP nanofibres) and the 615 nm emission peak (EDP nanofibres) were plotted against the sample configuration (differentiating between single layers; top layers, and bottom layers in the multilayer system). Fig. 5 [C] and [D] illustrate the variation in emission intensity for the TSP and EDP layers. The emission intensity of the emissive layer (either TSP or EDP) decreases when the layer placed below the top layer. This trend can be attributed to the multiple excitations experienced by the layer. When the layer is single with an aluminium substrate , the excitation light passes through the layer, reflects from the aluminium substrate, and reaches the top layer again, causing re-excitations. This results in the highest emission intensity for the single layer. In the multilayer system, the unabsorbed photons after exciting the first layer, encounter the second layer. The second layer absorbs some portion of the remaining excitation intensity subsequently emits. The unabsorbed light from second layer and emission from seond layers reflects back from the aluminium substrate. The single layer exhibits a higher emission intensity than the bilayer system in the top configuration.

4. Humidity sensing performance

Humidity sensing, the ability to measure and monitor the amount of moisture in the air, is essential in various applications due to its impact on human health, comfort, industrial processes, and more. The humidity sensitivity of the multilayer nanofibres system was examined for both the configurations. Both multilayer system configurations were excited at 320 nm as both top and bottom layers emits prominently at this common excitation wavelength. Due to significant emission at 320 nm, a large change in the intensity of the peaks with a slight change in percentage Relative humidity (% RH) can observed. The usefulness of the synthesised nanofibres as an opto-humidity sensor was tested in the multilayer nanofibres system under different relative humidity environments and its photoluminescence spectra were subsequently monitored. Several humidity environments were established in the chamber connected to the vacuum pump and spectrophotometer. According to

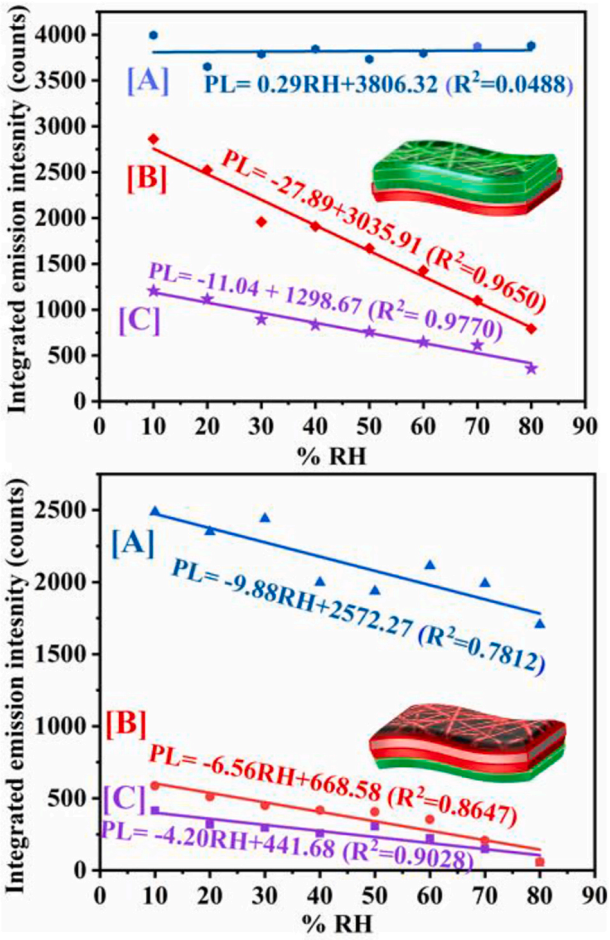

Fig. 9. Integrated peak area of multilayer system for configuration-1 (up) and configuration-2 (down) for the emission peaks [A] 615 nm, [B] 544 nm and [C] 490 nm.

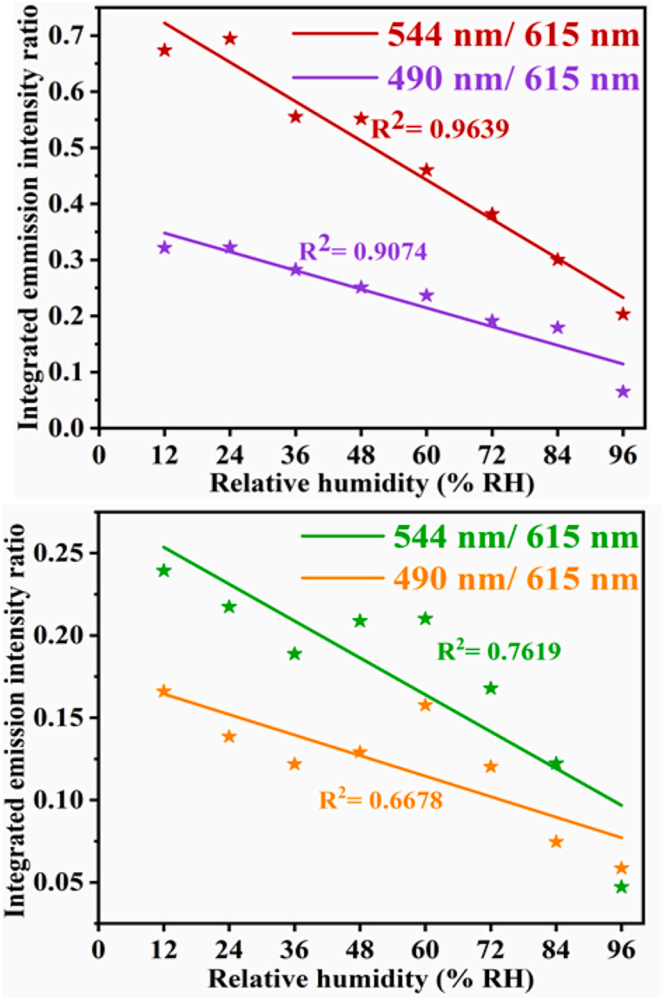

Fig. 10. Integrated peak area ratio of peaks of multilayer system when configuration-1 (up) and configuration-2 (down).

measurements that examined the luminescence of the nanofibres mat for a range of humidity values, the overall luminescence of the multilayer nanofibres system decreases significantly between 10 % and 80 % relative humidity (RH), regaining its initial value at 10 % relative humidity (Fig. 7). The effect of humidity was studied for the transitions $^5D_4 \rightarrow {}^7F_6$ (490 nm), $^5D_4 \rightarrow {}^7F_5$ (544 nm) of Tb^{3+} ion and $^5D_0 \rightarrow {}^7F_2$ (615 nm) of Eu^{3+} ion. The humidity effect on the multilayer nanofibres system was further studied by plotting the integrated peak emission intensity of the multilayer system for the two possible configurations. For both the configurations the Tb^{3+} ion emission peaks i.e., 490 nm and 544 nm show a gradual decrease in the Photoluminescence intensity with increasing % RH values between 10 % and 80 % respectively and vice-a versa. In case of configuration-01, for the RH values between 10 and 80 %, the emission intensity was significantly changed Δ~28 % (for 544 nm) and Δ~30 % (for 490 nm) giving quite good sensitivity. For configuration-02, the change in emission intensity with RH (unit%) was estimated to be ~8 (counts)/% RH and ~5(counts)/% RH. Considering the variation in emission peak intensity of 615 nm (Eu^{3+}) only a slightly variation was noticed for the two configurations. For both the configurations (01 and 02) it was observed that there was no major change in the emission intensity of peaks of Eu^{3+} ions with RH (unit%).

The emission spectra of the multilayer nanofibres system was qualitatively examined with increasing and decreasing RH (unit %) values by hysteresis curves. The hysteresis curves were plotted i.e. curve for integrated emission peak intensity Vs variation in RH (unit %) (for increasing and decreasing cycles) (Fig. 8). The analysis of hysteresis curves for the emission peaks 490 nm and 544 nm, reveals that both the curves following the same path; while for the 615 nm, disparity was observed at some points.

To investigate further, the humidity sensing performance curves were plotted for each peak's integrated emission intensities, and these were linearly fitted. It was observed that there was a good linear correlation between the highest PL intensity and the RH, implying that static quenching is dominant [25]. Fig. 9 shows the fitted curves of the emission peaks for the two configurations. It was observed that configuration-1 showed better linearity between the emission intensity of the peaks and % RH.

The ratiometric analysis of the emission peak intensities was also obtained for the multilayer nanofibres system (Fig. 10). To assess the humidity-sensing performance, the ratio of the Tb^{3+} emission intensity at peaks 544 nm and 490 nm to the emission peak of Eu^{3+} (615 nm) was calculated and plotted against relative humidity (% RH) values. This ratio was calculated relative to the relatively stable intensity of the 615 nm emission peak, as the luminescence intensity of the 544 nm and 490 nm peaks varies significantly with % RH. In general, the linear relationship between the integrated intensity ratio and relative humidity was observed. Hence, it can be deduced that the multilayer system can potentially be employed for ratiometric humidity sensing purposes. Among the two curves, the data for configuration-1 was better fitted to the linear curve.

The investigation of the cycle stability and response recovery times of the configuration-1 layer in the bilayer system was conducted to assess its practical usability, as it exhibited a good linear response of

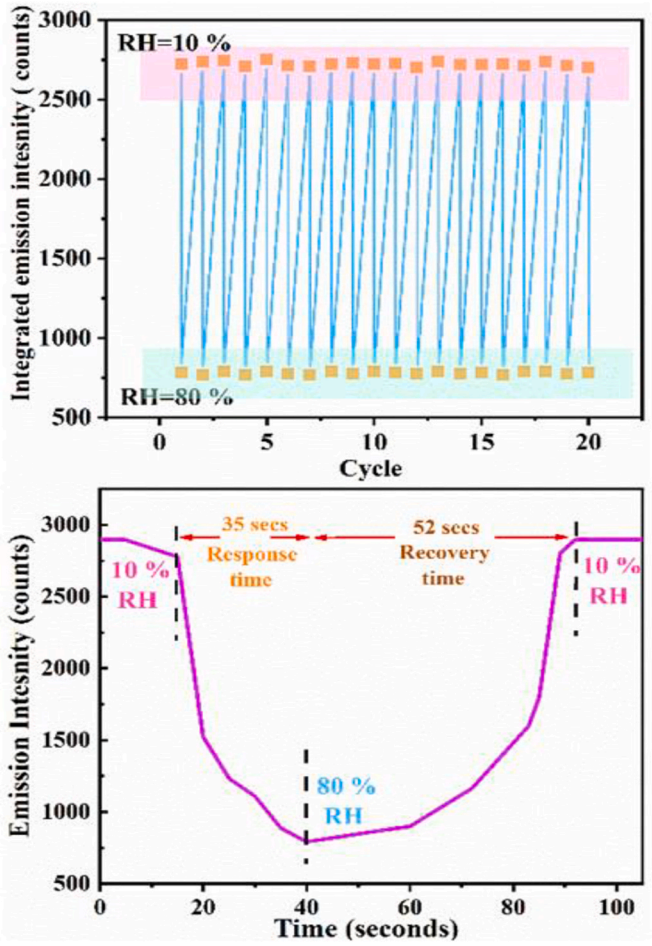

Fig. 11. The cyclic stability (up) and the response (down) as well as recovery time curves for configuration-1.

emission intensity across different % RH values. Cycle stability refers to the number of cycles up to which the nanofibres layer retains its luminescence intensity values. For this purpose, the nanofibres multilayer was exposed to cycles of varying %RH from 10%RH to 80%RH and the emission intensity was monitored. The curve was plotted for atleast 20 cycles (Fig. 11), showing major variations in the emission intensity of the multilayer nanofibres system. To check the cycle stability of the multilayer nanofibres layer, the emission peak intensity of the most linearly varying peak of the spectra, i.e., 544 nm, was plotted. The emission intensity does not vary significantly , thereby confirming the good cyclic stability of the multilayer nanofibres system.

Response and recovery durations may be ascertained by executing gradual variations to the RH and rapidly acquiring emission spectra at different time intervals until the emission intensity and wavelength stay constant. In situ, emission intensity (544 nm) was continuously observed until the emission intensity became constant for both increasing and falling RH values from 10 % to 80 % and 80 %–10 %, respectively, in order to quantify the response and recovery time dynamic. The intensity of the nanofibres in the vacuumed chamber (10 % RH) was measured to determine the response time. Further, humidity was introduced into the chamber via the pump to achieve 80 % RH values. The duration of this process was recorded until the emission intensity stabilised, which was determined to be 35 s. The chamber was then vacuumed once more in order to achieve a humidity level of 10 % RH. The recovery period, which was discovered to be 52 s, was measured from the moment the emisison intensity value became constant (Fig. 11). We keep the samples for more than one year to monitor any degradation in mat surface quality and emission characteristics under laboratory conditions. We do not find any obvious degradation either in the quality of the mat or any significant change in the emission intensity of the layers. However, due to the deposition of dust and air content, a mild surface-colour variation was observed. We expect the PVA mats to be durable when kept in closed or low-humidity environments. However, considering the ambience sensitivity of PVA towards humidity, it may degrade in an open environment, which is expected for long exposure.

The humidity sensing mechanism of the nanofibre layer was proposed on the basis of previous studies [7,26,27]. Because of the PVA polymer's hydrophilic nature, the PVA molecules are prone to interact with environmental water molecules more effectively. In addition, the large surface area of nanofibres for adsorption enhances the RH responsiveness. For the case of the lanthanide complex in PVA nanofibres, the primary cause of the reduction in emission is the rise in non-radiative relaxation brought on by higher humidity. The presence of high –OH content in the lattice induced higher non-radiative relaxation and cross-relaxation probability [28]. Notably, the Tb^{3+} and Eu^{3+} ions are enriched with large number of closely spaced energy levels, which facilitate the non-radiative cross-relaxation through transitions: $^5D_3(Tb^{3+}) + {}^7F_6(Tb^{3+}) \rightarrow {}^5D_4(Tb^{3+}) + {}^7F_0(Tb^{3+})$ [29] and $^5D_1(Eu^{3+}) + {}^7F_0(Eu^{3+}) \rightarrow {}^5D_0(Eu^{3+}) + {}^7F_1(Eu^{3+})$ [30] under suitable lattice phonon absorption.

5. Conclusions

A single layer and multilayer $Tb(Sal)_3Phen$ and $Eu(DBM)_3Phen$ incorporated PVA nanofibres were successfully fabricated. A good aspect ratio of the synthesised nanofibres (diameter ~273 ± 1.25 nm and ~148 ± 1.22 nm and length >1 mm for TSP and EDP, respectively) was reported. The emission intensity of the bilayers of nanofibres are found to be function of different layer configurations, leading to significant alteration in overall colour perception. The bilayer nanofibres system was reported having dual properties i.e. colour modulation and humidity sensing. The multilayer nanofibres showed excitation wavelength dependent colour modulation properties. Excitation wavelength and configurational scheme based colour modulation varying from blue green to red colour was observed. The emission intensity and intensity ratios (544nm/615 nm) linearly varied with RH. Results suggest that the bilayer nanofibres could be a suitable candidate for flexible fluorescent ratiometric moisture sensor. The opto-humidity response of bilayer nanofibres demonstrates a good optical response between relative humidity values of 10 % and 80 %. The bilayer nanofibres displayed acceptable response (35 s) and recovery durations (52 s) with good negligible hysteresis, and cyclic stability.

CRediT authorship contribution statement

Pooja: Methodology, Software, Writing – original draft, Visualization, Investigation, Validation. **Ketan Pancholi:** Writing – review & editing. **Yashashchandra Dwivedi:** Writing – review & editing, Validation, Supervision, Resources, Project administration, Investigation, Conceptualization.

Declaration of competing interest

The authors declare that they have no known competing financial interests or personal relationships that could have appeared to influence the work reported in this paper.

(Y. Dwivedi).

Data availability

Data will be made available on request.

Acknowledgements

Author (Pooja) acknowledge the financial assistance from Institute scholarship, National Institute of Technology Kurukshetra, India. Dr. Y. Dwivedi would like to acknowledge financial support from Project: HSCSIT/R&D/2022–2023/4508 from Haryana State Council for Science, Innovation and Technology, Directorate of Science and Technology, Haryana, India.

References

[1] Z. Ma, T. Fei, T. Zhang, An overview: sensors for low humidity detection, Sensor. Actuator. B Chem. 376 (2023) 133039.
[2] S. Mishra, A.K. Singh, Optical sensors for water and humidity and their further applications, Coord. Chem. Rev. 445 (2021) 214063.
[3] X. Cheng, Q. Zhao, D. Meng, X. Wang, J. Ma, J. Li, X. He, Chitosan/polyvinyl alcohol-based direction-controlled photo-humidity dual responsive membrane, ACS Appl. Polym. Mater. 4 (2021) 488–496.
[4] M. Hasegawa, H. Ohmagari, H. Tanaka, K. Machida, Luminescence of lanthanide complexes: from fundamental to prospective approaches related to water- and molecular-stimuli, J. Photochem. Photobiol. C Photochem. Rev. 50 (2022) 100484.
[5] F. Fueyo-González, E. Garcia-Fernandez, D. Martínez, L. Infantes, A. Orte, J. A. González-Vera, R. Herranz, Smart lanthanide antennas for sensing water, Chem. Commun. 56 (2020) 5484–5487.
[6] Y. Gao, P. Jing, N. Yan, M. Hilbers, H. Zhang, G. Rothenberg, S. Tanase, Dual-mode humidity detection using a lanthanide-based metal–organic framework: towards multifunctional humidity sensors, Chem. Commun. 53 (2017), 4468, 2017.
[7] Y. Dwivedi Pooja, Comparative spectroscopic study of Tb:Ce(Sal)3Phen complex inhibited PVA nanofibres for flexible moisture sensor, Spectrochim. Acta Part A Mol. Biomol. Spectrosc. 302 (2023) 123078.
[8] H. Zou, Y. Zhang, Z. Duan, Y. Tong, J. Peng, X. Zheng, Humidity sensing properties of LnFeO3 nanofibres synthesized by electrospinning (Ln=Sm, Nd, La), Mater. Res. Express 5 (2018) 015022.
[9] T. Delipinar, A. Shafique, M.S. Gohar, M.K. Yapici, Fabrication and materials integration of flexible humidity sensors for emerging applications, ACS Omega 6 (2021) 8744–8753.
[10] M. Venkatesan, L. Veeramuthu, F. Liang, W. Chen, C. Cho, C. Chen, J. Chen, Y. Yan, S. Chang, C. Kuo, Evolution of electrospun nanofibres fluorescent and colorimetric sensors for environmental toxicants, pH, temperature, and cancer cells–A review with insights on applications, Chem. Eng. J. 397 (2020) 125431.
[11] A. Bigdeli, F. Ghasemi, S. Abbasi-Moayed, M. Shahrajabian, N. Fahimi-Kashani, S. Jafarinejad, M.A.F. Nejad, M.R.H. Nezhad, Ratiometric fluorescent nanoprobes for visual detection: design principles and recent advances-a review, Anal. Chim. Acta 1079 (2019) 30–58.
[12] M.M. Memon, Q. Liu, A. Manthar, T. Wang, W. Zhang, Surface acoustic Wave humidity sensor: a review, Micromachines 14 (2023) 945.
[13] Y. Dwivedi, Surface Modification and (Bio) Functionalization of Upconverting Nanoparticles in Book Upconverting Nanoparticles: from Fundamentals to Applications, Wiley-VCH GmbH, 2022, pp. 241–265.
[14] S. Kano, N. Jarulertwathana, S.M. Noor, J.K. Hyun, R. Asahara, H. Mekaru, Respiratory monitoring by ultrafast humidity sensors with nanomaterials: a review, Sensors 22 (2022) 1251.
[15] Y. Dwivedi Pooja, Fabrication and spectroscopic investigations of green emitting $Tb(Sal)_3Phen$ complex embedded in polymer nanofibres, Appl. Phys. A 128 (2022) 870.
[16] P.S. Chowdhury, S. Saha, A. Patra, The role of semiconducting hosts on photoluminescence efficiency of Eu-complex, Chem. Phys. Lett. 405 (2005) 393–397.
[17] M.K. Trivedi, A.B.D. Trivedi, H.S.K. Bairwa, Fourier transform infrared and ultraviolet-visible spectroscopic characterization of biofield treated salicylic acid and sparfloxacin, Nat. Prod. Chem. Res. 3 (2015) 186.
[18] G.F. Diaza, M.M.C. Valletteb, M.S. Saavedraa, R.E. Clavijoa, J.C. Canalesa, J. Costamagnac, J. Vargasd, Surface vibrational study of macrocycle complexes: Co (II), Ni(II), Cu(II) and Zn(II) bis(phenylhydrazine)-1,10-phenanthroline, Vib. Spectrosc. 28 (2002) 223–234.
[19] G. Kaur, Y. Dwivedi, S.B. Rai, Synthesis, structural, thermal and optical studies of rare earth coordinated complex: $Tb(Sal)_3Phen$, Mater. Chem. Phys. 130 (2011) 1351–1356.
[20] I.M. Jipa, A. Stoica, M. Stroescu, L. Dobre, T. Dobre, S. Jinga, C. Tardei, Potassium Sorbate Release from Poly(vinyl Alcohol)-Bacterial Cellulose Films, vol. 66, 2012, pp. 138–143.
[21] H. Yu, T. Li, B. Chen, Y. Wu, Y. Li, Preparation of aligned $Eu(DBM)_3phen$/PS fibers by electrospinning and their luminescence properties, J. Colloid Interface Sci. 400 (2013) 175–180.
[22] I. Malina, N. Juhnevics, V. Kampars, Study of thermal and optical properties of dibenzoylmethane Eu (III) organic complexes, Proc. Est. Acad. Sci. (2017) 493–500.
[23] M.O. Iwunze, Absorptiometric determination of acetylsalicylic acid in aqueous ethanolic solution, Anal. Lett. 41 (2008) 2944–2953.
[24] G. Nitulescu, D. Lupuliasa, I. Adam-Dima, G.M. Nitulescu, Ultraviolet filters for cosmetic applications, Cosmetics 10 (2023) 101.
[25] B.B. Purdy, R.J. Hurtubise, Mechanistic aspects of moisture quenching in solid-matrix luminescence with phenylphenols adsorbed on filter paper, Anal. Chem. 64 (1992) 1400–1404.
[26] W. Zhang, J. Xie, Z. Sui, Z. Xu, X. Wang, M. Lei, H. Zhang, Z. Li, Y. Wang, W. Liu, W. Du, S. Wang, Ratiometric recognition of humidity by a europium-organic framework equipped with quasi-open metal site, Sci. China Chem. 64 (2021) 1723–1729.
[27] D. Xia, J. Li, W. Li, L. Jiang, G. Li, Lanthanides-based multifunctional luminescent films for ratiometric humidity sensing, information storage, and coloured coating, J. Lumin. 231 (2021) 117784.
[28] G. Lakshminarayana, E.M. Weis, A.C. Lira, U. Caldino, D.J. Williams, M.P. Hehlen, Cross relaxation in rare-earth-doped oxyfluoride glasses, J. Lumin. 139 (2013) 132–142.
[29] C.K. Duan, C.C. Ko, G. Jia, X. Chen, P.A. Tanner, 5D3–5D4 cross-relaxation of Tb3+ in a cubic host lattice, Chem. Phys. Lett. 506 (2011) 179–182.
[30] Y. Dwivedi Rashmi, Dual interactions and thermo-optical analysis of YAGG:Ce/Eu nanophosphor, Spectrochim. Acta, Part A 254 (2021) 119679.